Materials and Design 31 (2010) 4866–4875

Contents lists available at ScienceDirect

Materials and Design

journal homepage: www.elsevier.com/locate/matdes

Short Communication

Experimental and numerical evaluation of forming limit diagram for Ti6Al4V titanium and Al6061-T6 aluminum alloys sheets

F. Djavanroodi *, A. Derogar

Mechanical Engineering Department, Iran University of Science and Technology, Tehran, Iran

ARTICLE INFO

Article history:
Received 14 November 2009
Accepted 15 May 2010
Available online 21 May 2010

ABSTRACT

The forming limit diagram (FLD) is a useful concept for characterizing the formability of sheet metal. In this work, the formability, fracture mode and strain distribution during forming of Ti6Al4V titanium alloy and Al6061-T6 aluminum alloy sheets has been investigated experimentally using a special process of hydroforming deep drawing assisted by floating disc. The selected sheet material has been photo-girded for strain measurements. The effects of process parameters on FLD have been evaluated and simulated using ABAQUS/Standard. Hill-swift and NADDRG theoretical forming limit diagram models are used to specify fracture initiation in the finite element model (FEM) and it is shown that the Hill-swift model gives a better prediction. The simulated results are in good agreement with the experiment.

1. Introduction

In recent years there has been growing demand for the production of hydroformed parts. Hydroforming of sheet metal makes use of hydraulic pressure to improve the basic deep drawing process. Hydroforming generally increases the draw ratio and minimizes the thickness variation of the formed part; in addition, other advantages associated with it are: requiring only one rigid tool and subsequently improving the quality of the products which as a result, lighter, cheaper, stronger, stiffer and less springback components are produced. Disadvantages include slow cycle times, highly polished dies and requirement of punch stroke/fluid pressure path characteristic to minimize wrinkling and rupturing occurrence [1–5].

Titanium alloy and aluminum alloy sheets are widely used in the automotive and aerospace industries due to continuous demands for the use of lightweight materials. During forming, these sheets are subjected to various types of strain. When the strain reaches/exceeds a critical value, different types of failures namely necking, fracture and wrinkling [6,7] occur.

Forming limit diagram provides the limiting strains a sheet metal can sustain whilst being formed. Laboratory testing has shown that lubrication, sheet curvature, thickness, orientation and material properties have effects on FLD [8–11]. The FLD is very useful in FEM analysis, die design optimization, die tryout, and quality control during production [12]. In recent years many techniques have been developed to evaluate FLD experimentally [13–16]. These include elimination of frictional effects between tool and material, the flatness of the blank surface and using parameters obtained from conventional tensile testing to determine FLD.

Moreover, with the increase of computational techniques, several researchers have proposed numerical models to predict the FLDs. Ductile fracture criterion to predict the forming limits was used. Based on these criteria, the occurrence of ductile fracture is estimated using the macroscopic stress and strain that occurs during deformation [17–20]. Other models have also been proposed: diffuse necking by Swift [21], localized necking introduced by Hill [22], the thickness imperfection model developed by Marciniak and Kuczynski [23] and the vertex theory brought forward by Stren and Rice [24]. However, predicting the FLD requires complex calculations and this will limit their use in practical applications. Furthermore, a general model that can be applied for various sheet metals has not been proposed.

In this paper, a new hydroforming die, assisted by a floating disc which combines hydrodynamic deep drawing and viscose pressure forming is used. With this new arrangement the normal blank holding force and chamber pressure will be halved, and the punch force has been decreased. Uniaxial tension tests were used to obtain material properties. For a better understanding of the forming behavior of these materials FLD diagrams for Ti6Al4V alloy and Al6061-T6 alloy sheets have been studied. The effects of process parameters on FLD diagram have been evaluated and simulated using ABAQUS/Standard. Hill-Swift [25] and NADDRG [26] theoretical forming limit diagram models are used to specify fracture initiation in the finite element model and it is shown that the Hill-Swift model gives a better prediction.

* Corresponding author. Tel./fax: +98 21 77240203.
E-mail address: javanroodi@iust.ac.ir (F. Djavanroodi).

0261-3069/$ - see front matter © 2010 Elsevier Ltd. All rights reserved.
doi:10.1016/j.matdes.2010.05.030

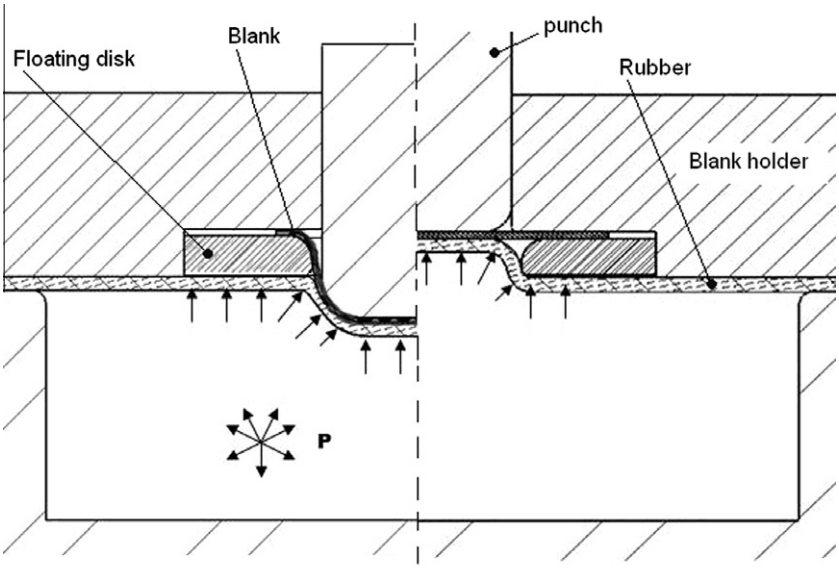

Fig. 1. The hydroforming process assisted by floating disk.

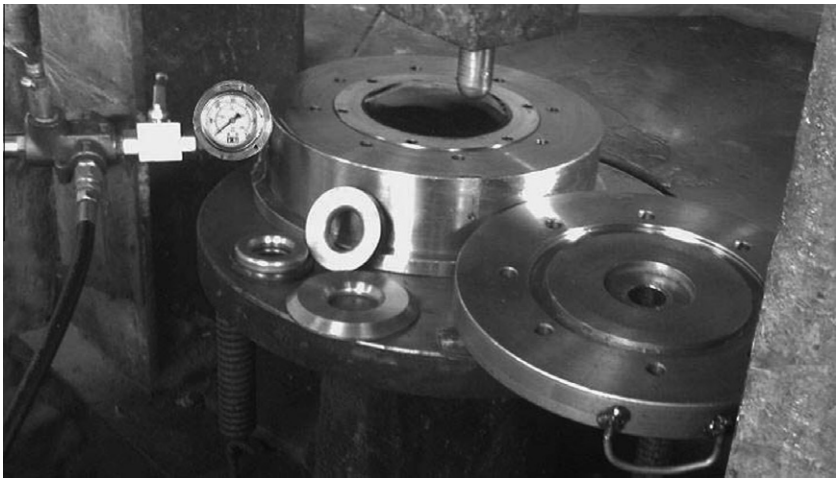

Fig. 2. Hydraulic press & die.

2. Experimental procedure

2.1. Hydroforming die

Hydroforming assisted by a floating disc is a new method that can simplify the tools used for hydroforming and decrease the cost of the process. With a floating disk, two sides of a blank will suffer equal friction force due to the normal blank holding force, in contrast to hydrodynamic deep drawing and viscose pressure forming processes, in which the medium in the chamber is in contact with one side of the blank. Therefore, the normal blank holding force and chamber pressure will be halved, and the punch force can consequently be decreased. Moreover, the die is very simple. The need for an independent hydraulic system to control the blank holding force and a complicated control system to adjust the gap between the die and blank holder can be avoided.

Fig. 1 shows the tools used. These are; punch, blank holder, pressure chamber, rubber diaphragm and floating disk. The diaphragm and the disk at the bottom can move up and down due to the pressure of the viscous medium in the chamber. The blank is placed between the blank holder and the floating disk. The blank holding force (BHF) due to the pressure of the chamber and the area of the floating disk can press the blank tightly to the blank holder. As the punch moves down, the process starts. A control valve regulates the liquid flow and the blank holding force can consequently be controlled.

All of the experiments were carried out using a 250-ton hydraulic double-action press. Fig. 2 shows the equipment used and Table 1 gives the dimensions of the tools used for this process. For

Table 1
Tool dimensions.

Parameters (mm)	Values
Punch diameter, d	40
Inside die (disk) diameter, d_d	43.5
Punch nose radius, r_p	10
Die entrance radius, r_{die}	5
Inside blank holder diameter, d_c	40.2
Blank holder entrance radius, R_c	2

supplying oil to the container pressure, a hydraulic pump with maximum pressure up to 500 bar is used.

The blank is lubricated with common grease on both sides and placed between disk and blank holder and centered. Pressure in the cavity is gradually raised to form the blank upward in the reverse direction (PPB). The rigid punch moves down into the fluid chamber and the blank is forced to assume the shape of the punch.

2.2. Tensile test

The materials used in this investigation are Ti6Al4V titanium and Al6061-T6 aluminum alloy sheets, with the thickness of 1.08 mm and 0.8 mm respectively. Table 2 displays the properties for these materials obtained from uniaxial tensile testing based on ASTM E8 standard and anisotropic characteristics (r-values) obtained according to ASTM-E517 standard. The tests were conducted along three directions, with the tensile axis being parallel (0°), diagonal (45°) and perpendicular (90°) to the rolling direction of the sheet. A constant cross-head speed of 0.1 mm min^{-1} was employed in all cases.

2.3. FLD test

Empirical FLDs evaluated using Hecker's simplified technique [13]. In this method, the experimental procedure mainly involves three stages: grid marking the sheet specimens, punch-stretching the grid-marked samples to failure or onset of localized necking, and measurement of strains. The circles on the sheet samples became ellipses after deformation, falling into safe (forming is completed and without any problem), necked (near the crack region), wrinkle (located on the left side of the diagram), and failed (right side is related to initial fracture in punch radius zone and the left side is related to final fracture in flange zone) zones. Finally, FLD was drawn by plotting the minor strain along the abscissa and the corresponding major strain along the ordinate and by drawing a curve which separates the safe region from the unsafe region. The results are presented in Figs. 3 and 4 for Ti and Al alloys respectively. Using these figures the relative proximity of fracture or wrinkling can be determined and forming conditions can be selected accordingly. The strain combinations above and below the FLD line will lead to fracture and wrinkles respectively [10].

Table 2
Properties of sheet materials.

Parameters	Angle to rolling direction Ti6Al4V titanium alloy			Angle to rolling direction Al6061 aluminum alloy		
	0°	45°	90°	0°	45°	90°
Density (g/cm^3)	4.43			2.70		
Poisson's ratio	0.342			0.33		
Yielding stress (MPa)	544	544	558	305	302	300
Ultimate tensile stress, (MPa)	632	632	607	346	342	341
Total elongation (%)	30.7	30.7	27.2	19	18	19
Anisotropy factor (r)	2.4644	2.4644	4.1218	0.48	0.7	0.53
Strain-hardening exponent (n)	0.151	0.151	0.134	0.17	0.18	0.16
Hardening coefficient, k (MPa)	975	975	912.5	570	550	549
Average strain-hardening exponent (n)	0.15			0.17		
Average hardening coefficient, k (MPa)	959.4			554.7		
Average Anisotropy factor (r)	2.89			0.60		

Average = $(X_o + 2X_{45} + X_{90})/4$ where X is n or k-value or r-values [10].

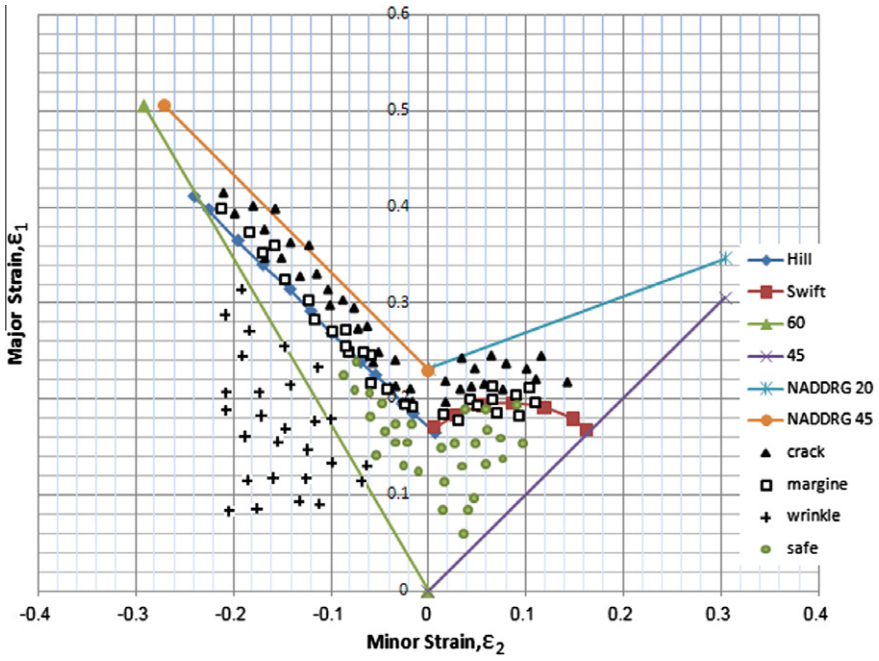

Fig. 3. Experimental FLD for Ti6Al4V alloy sheet.

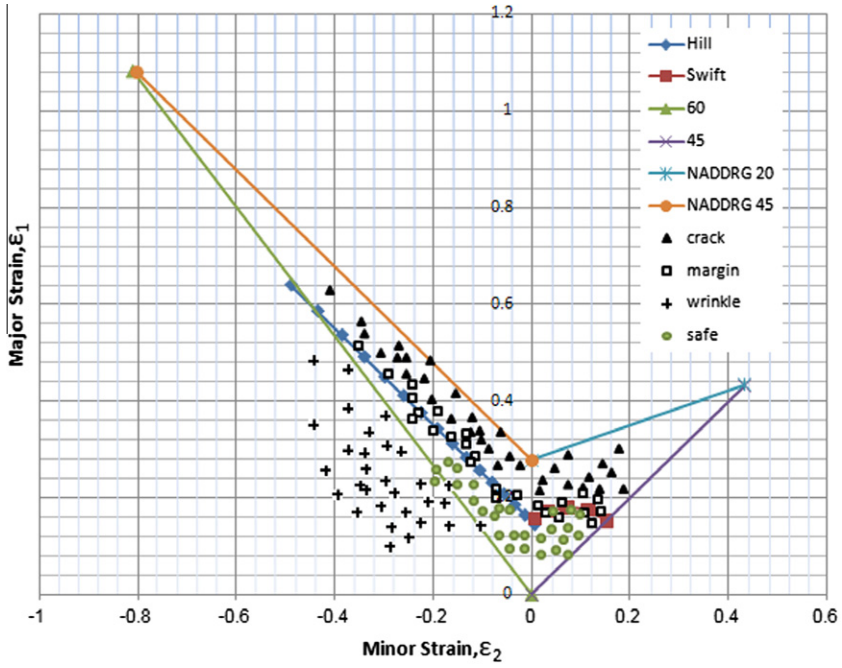

Fig. 4. Experimental FLD for Al6061-T6 alloy sheet.

3. FEM analysis

Explicit finite element code was used to simulate the process. Due to the symmetric character of the forming, only a quarter of the model was used. All die tools were assumed to be rigid, and the materials were modeled using S4R (a 4-node quadrilateral in-plane general-purpose shell with reduced integration) elements for fracture prediction and C3D8R (an 8-node linear brick with reduced integration) elements for modeling anisotropic effects in sheets. Mesh size is 0.5 mm and penalty contact interfaces were used to enforce the intermittent contact and the sliding boundary condition between the blank and the tooling elements. The material parameters used for the blank derived from the tensile test as shown in Table 2. Material constants (F, G, H, N, L and M) in Hill48 yield function [22] were calculated using anisotropy calculated according to ASTM-E517.

$$f(\sigma)=\sqrt{\mathrm{F}(\sigma_{22}-\sigma_{33})^2+\mathrm{G}(\sigma_{33}-\sigma_{11})^2+\mathrm{H}(\sigma_{11}-\sigma_{22})^2+2\mathrm{L}\sigma_{23}^2+2\mathrm{M}\sigma_{31}^2+2\mathrm{L}\sigma_{12}^2} \tag{1}$$

where σ_{ij} denotes the stress components. Material constants can be expressed in terms of six yield stress ratios R_{11}, R_{22}, R_{33}, R_{12}, R_{13} and R_{23} according to Eq. (2).

$$\begin{aligned}
\mathrm{F}&=\frac{1}{2}\left(\frac{1}{R_{22}^2}+\frac{1}{R_{33}^2}-\frac{1}{R_{11}^2}\right),\\
\mathrm{G}&=\frac{1}{2}\left(\frac{1}{R_{11}^2}+\frac{1}{R_{33}^2}-\frac{1}{R_{22}^2}\right),\\
\mathrm{H}&=\frac{1}{2}\left(\frac{1}{R_{11}^2}+\frac{1}{R_{22}^2}-\frac{1}{R_{33}^2}\right),\\
\mathrm{L}&=\frac{3}{2R_{23}^2},\quad \mathrm{M}=\frac{3}{2R_{13}^2},\quad \mathrm{N}=\frac{3}{2R_{12}^2}
\end{aligned} \tag{2}$$

$$R_{11}=R_{13}=R_{23}=1,\quad R_{22}=\sqrt{\frac{r_{90}(r_0+1)}{r_0(r_{90}+1)}},\\
R_{33}=\sqrt{\frac{r_{90}(r_0+1)}{r_{90}+r_0}},\quad R_{12}=\sqrt{\frac{3r_{90}(r_0+1)}{(2r_{45}+1)(r_{90}+r_0)}} \tag{3}$$

To determine location of fracture in the FEM model, FLD data was applied to software indirectly based on NADDRG, Hill-Swift model by user subroutine. Eqs. (4)–(7) shows the Hill-Swift model for calculating the forming-limit strains [25].

For $\varepsilon_2<0$: $\alpha=\sigma_2/\sigma_1$

$$\varepsilon_{j1}=\frac{1+(1-\alpha)r}{1+\alpha}n \tag{4}$$

$$\varepsilon_{j2}=\frac{\alpha-(1-\alpha)r}{1+\alpha}n \tag{5}$$

For $\varepsilon_2>0$:

$$\varepsilon_{f1}=\frac{[1+r(1-\alpha)].\left[1-\frac{2r}{1+r}\alpha+\alpha^2\right]}{(1+\alpha)(1+r).\left[1-\frac{1+4r+2r^2}{(1+r)^2}\alpha+\alpha^2\right]}\cdot n \tag{6}$$

$$\varepsilon_{f1}=\frac{[(1+r)\alpha-r].\left[1-\frac{2r}{1+r}\alpha+\alpha^2\right]}{(1+\alpha)(1+r).\left[1-\frac{1+4r+2r^2}{(1+r)^2}\alpha+\alpha^2\right]}\cdot n \tag{7}$$

Eq. (8) shows NADDRG model for calculating the forming-limit strains [26]. The slope of the lines located on the left and right sides of FLD are about 45° and 20°.

$$Fld_o=\frac{(23.3+14.13t_0)n}{0.21} \tag{8}$$

The strains which are measured in necking locations (ε_1, ε_2) are used in order to obtain FLD diagrams.

4. Results and discussion

4.1. Pressure curves

Figs. 5 and 6 show the chamber pressure versus the punch stroke using punch nose radii of 10 mm for limit drawing ratio $(LDR)_{Ti}$ of 2.25 and $(LDR)_{Al}$ of 2.0. Eq. (4) (the punch force that causes shearing of the blank) and Eq. (5) (the blank holding force by the fluid pressure acting on a flange area, e.g., the die contacting area) were used to obtain the approximate minimum and maximum limits of the initial pressure [27].

$$F_{punch} = \pi d t \frac{\sigma_y}{\sqrt{3}} \tag{9}$$

$$F_{flange} = p_{req} \frac{\pi}{4}(D'^2 - d'^2) \tag{10}$$

where D' is the blank diameter, d is the diameter of the blank contact region with the punch at the initial stage, d' is the inside

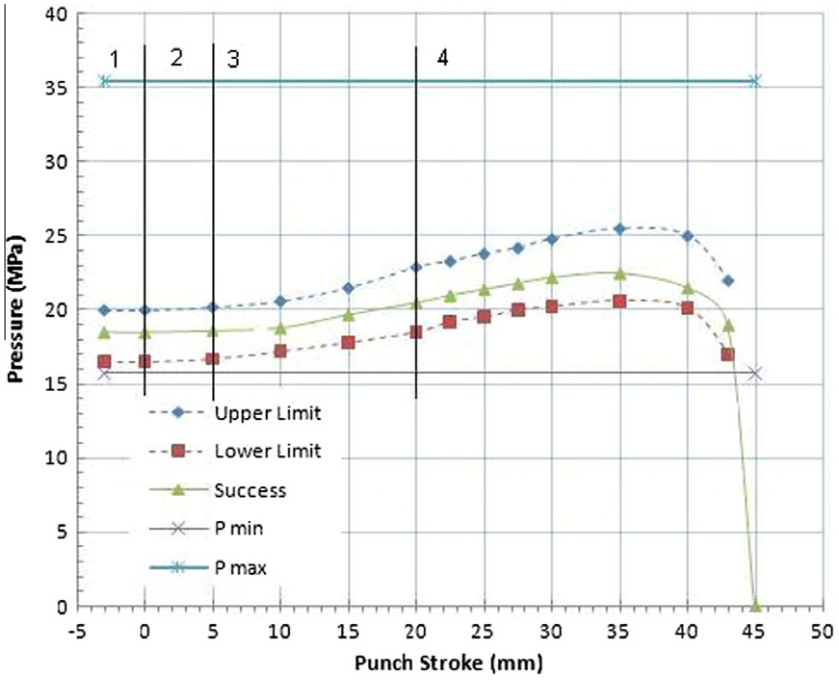

Fig. 5. Pressure-punch stroke curves for Ti6Al4V alloy sheet.

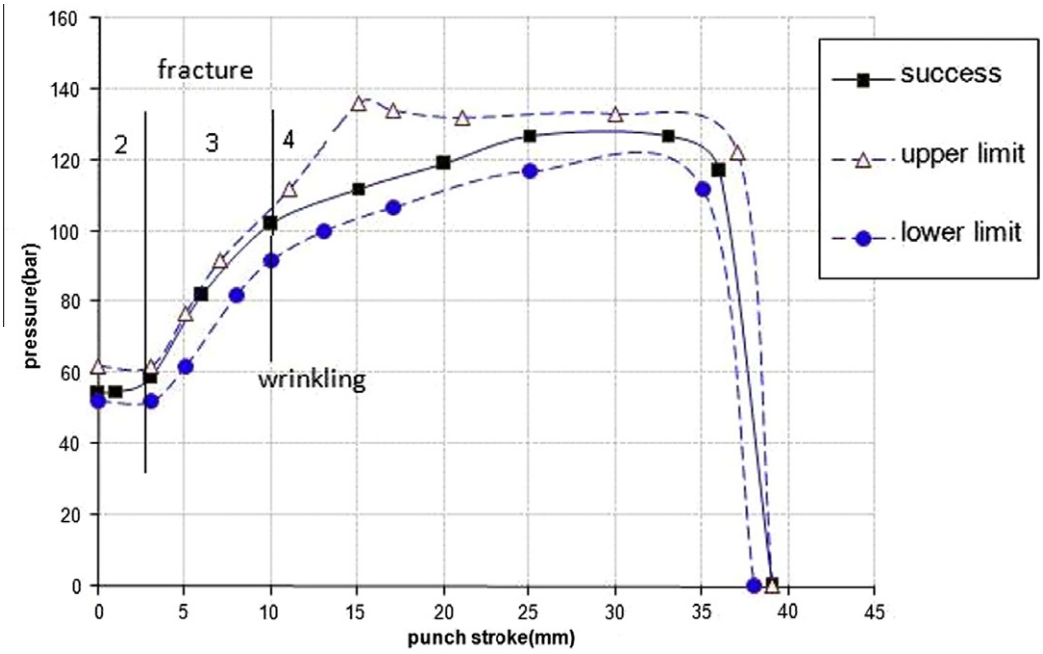

Fig. 6. Pressure-punch stroke curves for Al6061-T6 alloy sheet.

diameter of the disc, t is the blank thickness, σ_y is the tensile yield stress of the blank material and p_{req} is the required initial pressure. If the suppressing force due to fluid pressure is less than the punch force, then the blank tends to lift up. The suppressing force due to the fluid pressure should be higher than the punch force for a stable start of the process, $F_{flange} > F_{punch}$. Hence, the minimum required initial pressure becomes;

$$P_{req} = \beta \frac{4d \cdot t \cdot \sigma_y}{(D'^2 - d'^2)\sqrt{3}} \tag{11}$$

where β is the correction factor to compensate for forming difficulty due to the shape of the cross-section: for a circular section, $1 \leqslant \beta \leqslant 2$ [14]. Pressure in the die cavity can be divided into four zones as shown in Figs. 5 and 6: Zone 1 is pre-bulging, where the blank will be bulged 3 mm in the reverse direction; Zone 2 is the important stage where the initial pressure is applied – parameters can be calculated theoretically as mentioned before; Zone 3 is where the pressure increases with a sharp slope in comparison with the other zones; Zone 4 is the control zone. Finally, the liquid pressure decreases rapidly and is released because the entire flange has

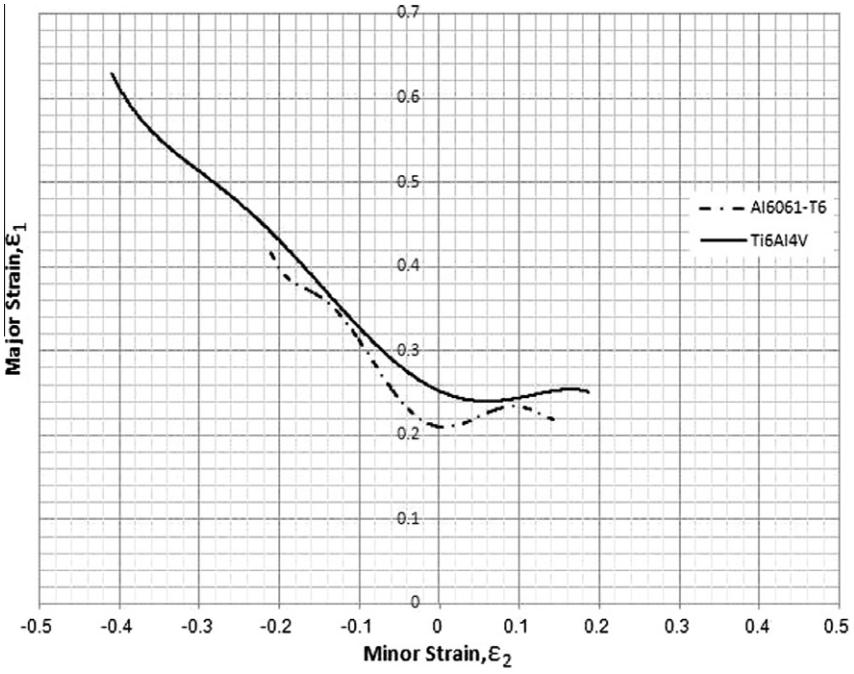

Fig. 7. Experimental FLDs for two alloys.

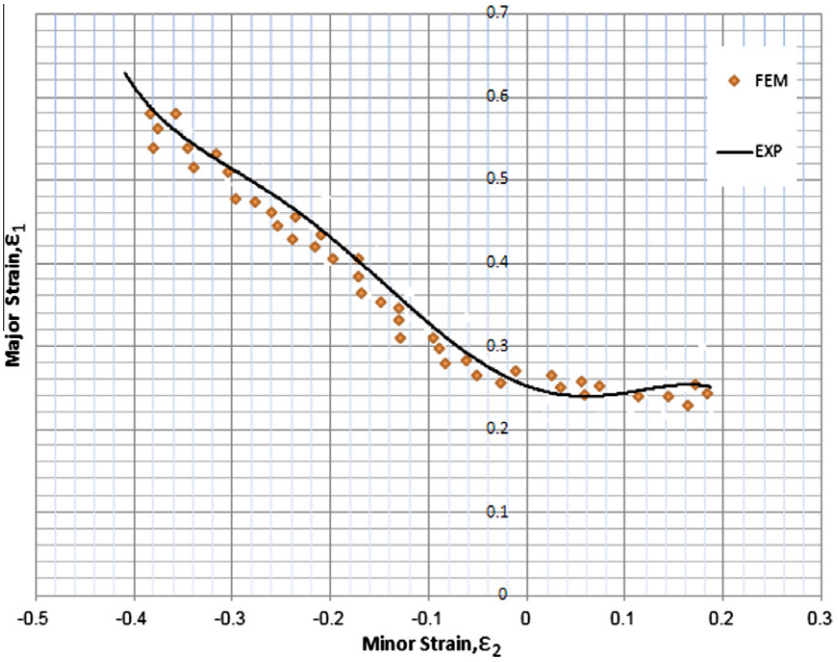

Fig. 8. Experimental versus numerical FLDs for Ti6Al4V alloy sheet.

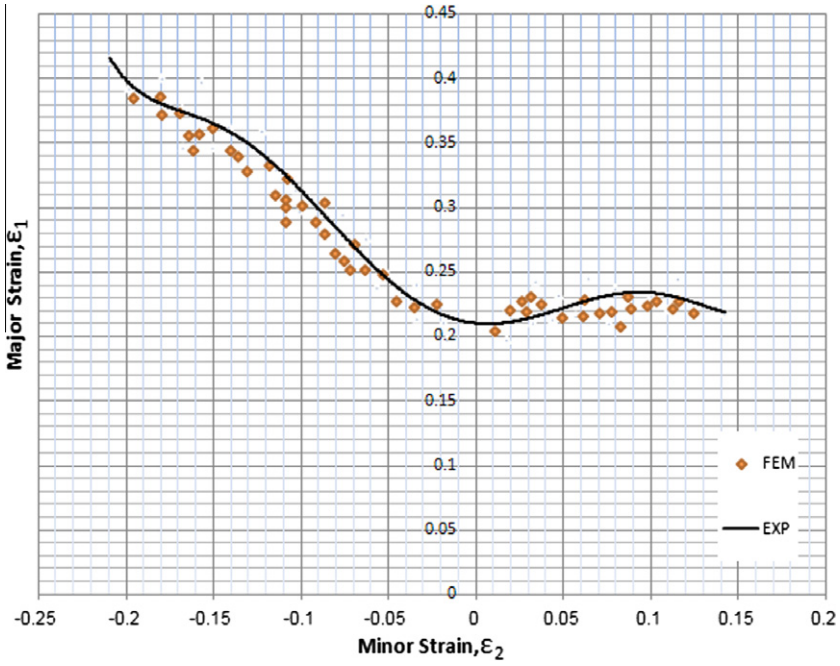

Fig. 9. Experimental versus numerical FLDs for Al6061-T6 alloy sheet.

been pulled into the die cavity. As shown, high fluid pressure causes excessive thinning of the sheet metal which will leads to premature rupturing. However, if the fluid pressure is too low, the sheet may not stretch enough during the process and will wrinkle. There is, therefore, an upper and lower limit on the fluid pressure related to the punch stroke as shown in Figs. 5 and 6. An optimum fluid pressure–punch stroke band exist which ensures limited rupturing and wrinkling failures of the finished part [3–5].

4.2. Tensile properties

The plastic strain values and normal anisotropy determined from tensile testing experiment for titanium and aluminum alloy sheets are tabulated in the Table 2. The titanium alloy shows a maximum n-value along rolling direction and minimum n-value along a 90° orientation to the rolling direction. For the same alloy, k-value is maximum along rolling direction and minimum along 90° orientation to the rolling direction. The aluminum alloy shows a maximum n-value along a 45° direction to the rolling direction and minimum along a 90° direction to the rolling direction. k-value is maximum along rolling direction and minimum along 90° direction to the rolling direction, as shown in Table 2. The average n-values of titanium and aluminum alloys are 0.15 and 0.17 respectively. A higher (n) value indicates better stretchability and formability [10]. The titanium alloy exhibits a maximum r-value along a 90° orientation to the rolling direction and a minimum r-value along rolling direction. The aluminum alloy exhibits a maximum r-value along 45° orientation to the rolling direction and a minimum r-value along the rolling direction. The average r-values of titanium and aluminum alloys are 2.89 and 0.6 respectively. A higher r-value indicates better resistance to thinning in the thickness direction during drawing [10].

Fig 7 shows influences of n- and r-values on the experimental FLDs. As discussed, a higher strain-hardening exponent (n) delays the onset of instability until the higher strain value, is reached and this delay enhances the limiting strain. Also, increasing plastic strain ratio (r) results in an increase of the formability of sheet material [10,11]. Fig. 7 shows that the forming limit curves for Ti

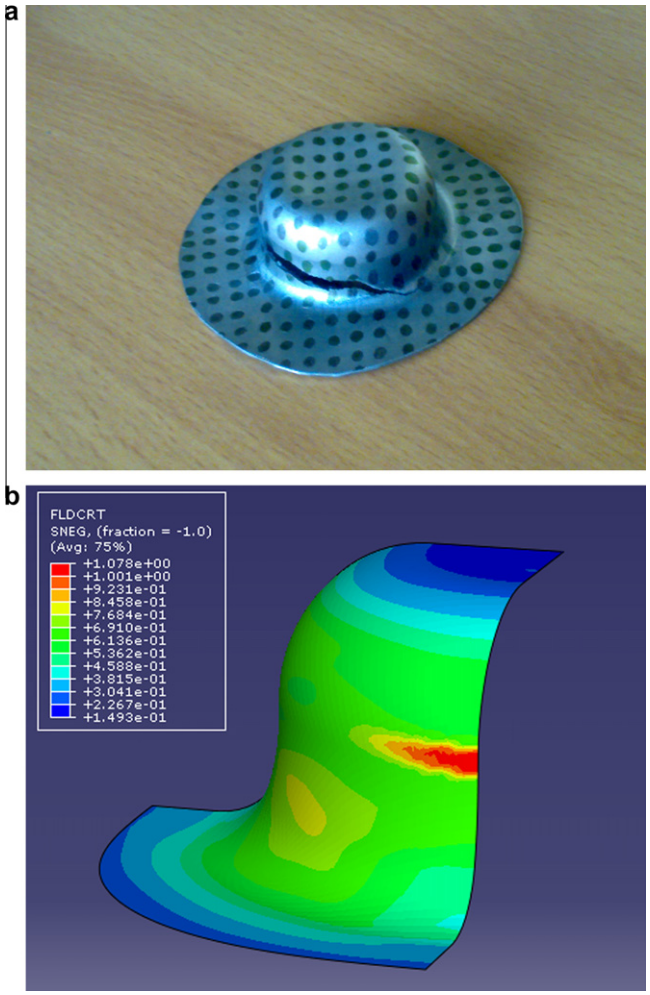

Fig. 10. Initial fracture mode in Ti6Al4 V alloy sheet (a) experiment, (b) simulation.

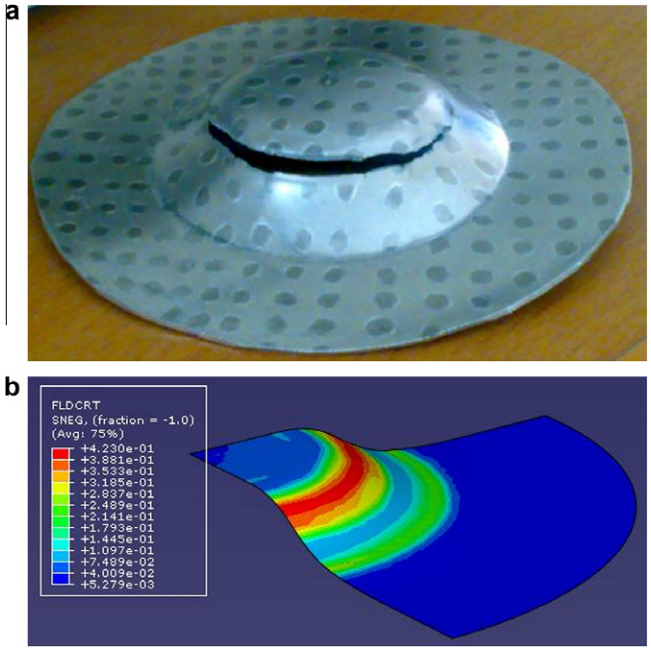

Fig. 11. Initial fracture mode in Al6061-T6 alloy sheet (a) experiment, (b) simulation.

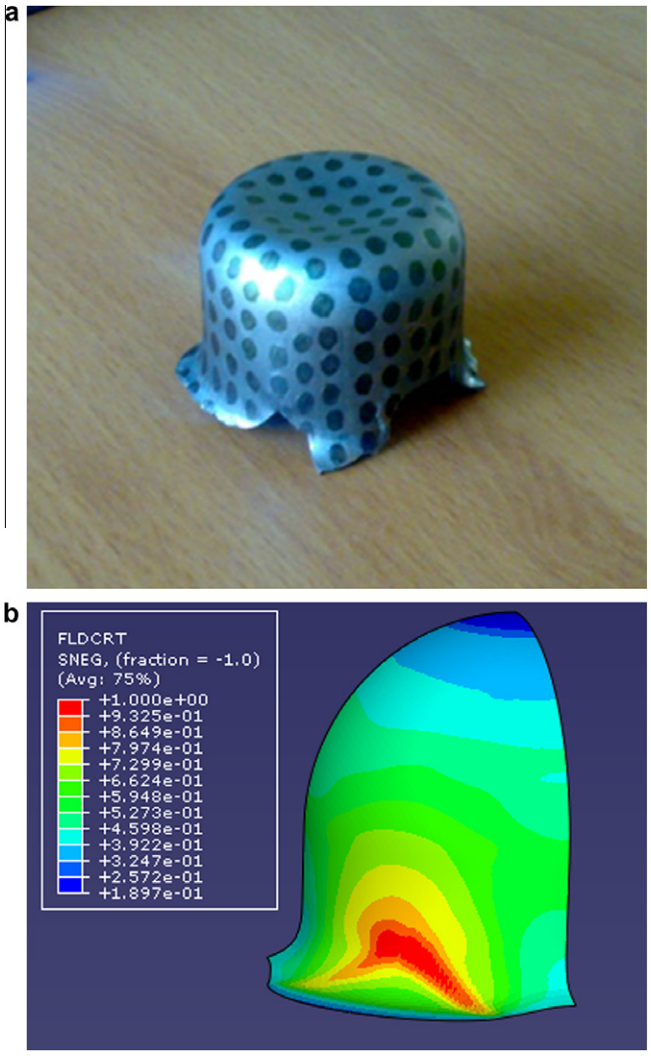

Fig. 12. Final fracture mode in Ti6Al4 V alloy sheet (a) experiment, (b) simulation.

alloy is higher than Al alloy. This is because Al alloy has a slightly higher value of the strain-hardening exponent, but Ti alloy has much larger plastic strain ratio (r) values.

4.3. Comparison between theoretical and experimental FLDs

The comparisons between experimental and theoretical FLDs are shown in Figs. 8 and 9. Two types of finite element models were used for this study: quarter- and full-model. The anisotropy parameters r_0, r_{45} and r_{90} used for modeling the data, are determined from tensile tests experimentation performed in 0°, 45° and 90° measured from the rolling direction of the sheets. Hill-Swift [25] and NADDRG [26] theoretical forming limit diagram models are used to specify fracture initiation in the finite element model, and it is seen that the Hill-Swift model gives a better prediction. A good agreement has been obtained between experimental and simulated model for 10 mm dies radius as shown in Figs. 8 and 9.

4.4. Failure mode prediction

In general, the failure modes can be divided into two types: wrinkling and fracture. Figs. 10–15 show these failures and prediction of these failure modes by the simulation for these two alloys.

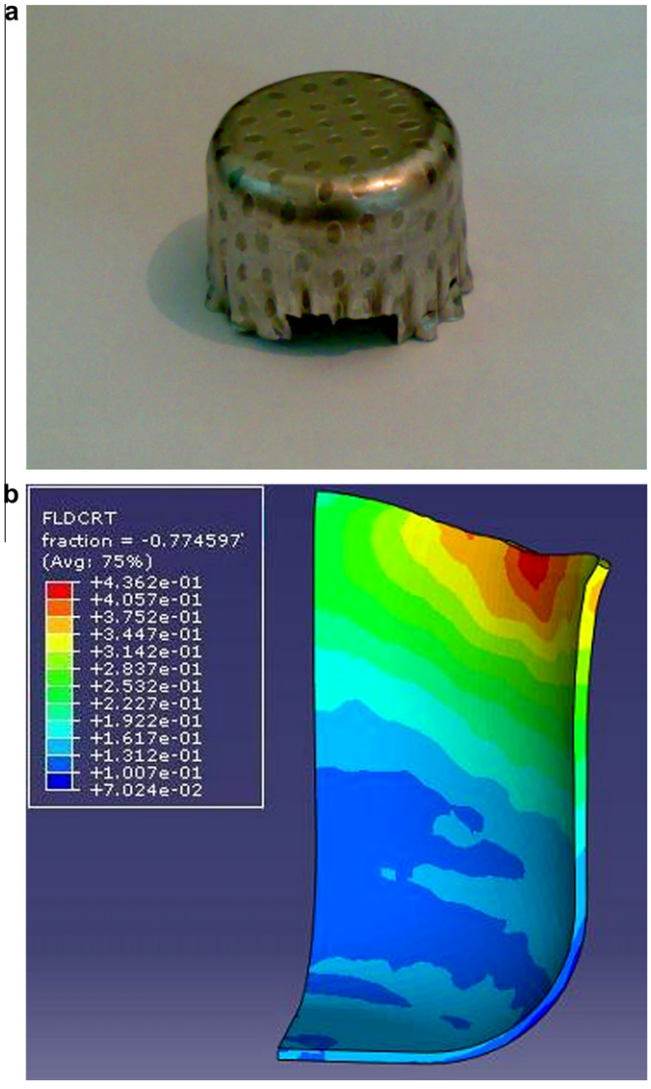

Fig. 13. Final fracture mode in Al6061-T6 alloy sheet (a) experiment, (b) simulation.

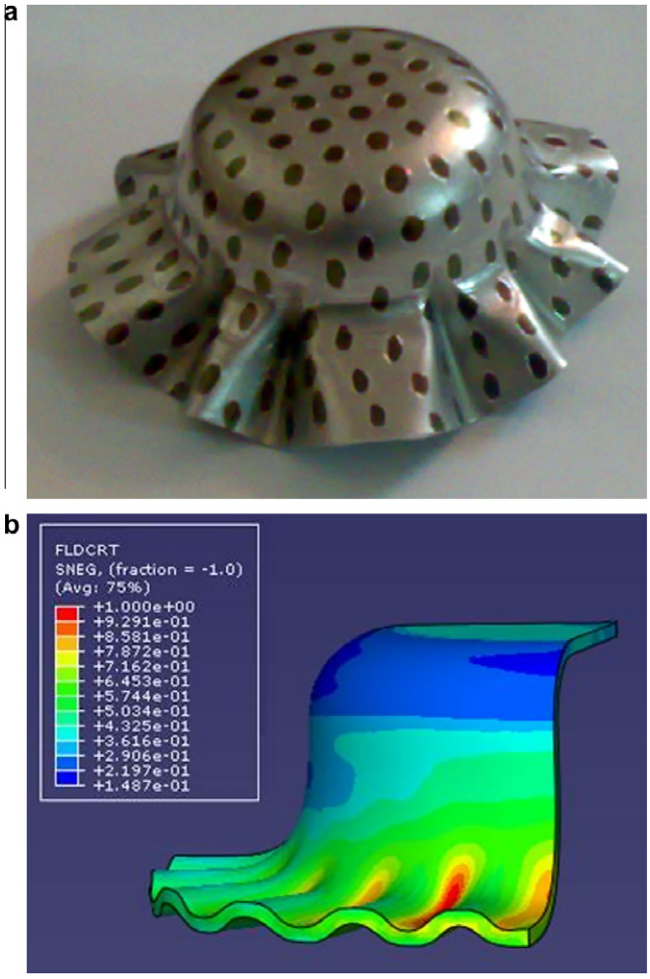

Fig. 14. Wrinkle mode in Ti6Al4V alloy sheet (a) experiment, (b) simulation.

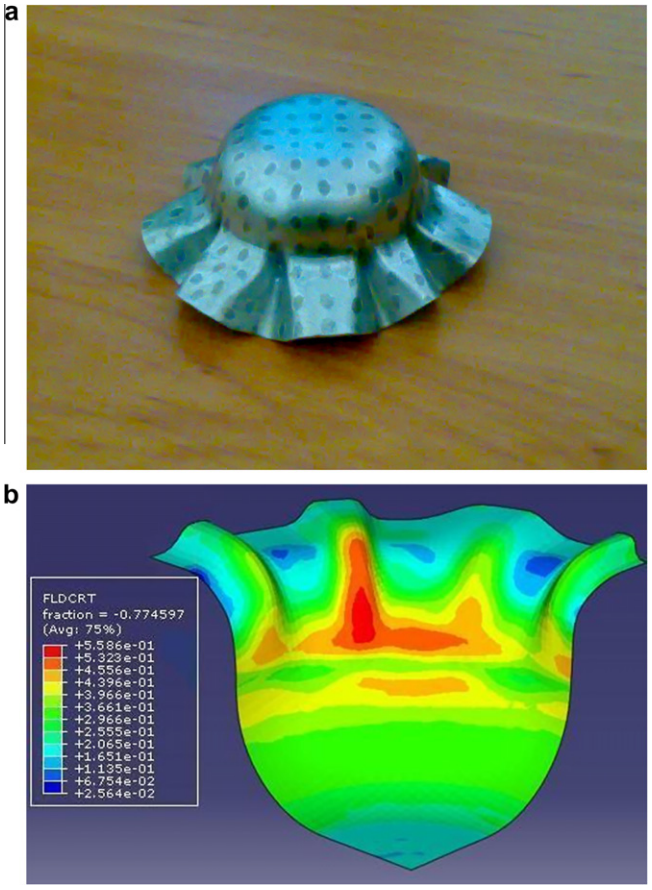

Fig. 15. Wrinkle mode in Al6061-T6 alloy sheet (a) experiment, (b) simulation.

In the experiment two types of fracture have been recorded, as shown in Figs. 10–13: the initial fracture and final fracture. The initial fracture is caused mainly by insufficient initial liquid pressure, poor lubrication and too large drawing ratio. The final fracture mode arises because of the too large bending and unbending effects at the floating disk. Decreasing the liquid pressure at the final stage and use of a good lubricant on the flange can prevent final fracture. The initial failure results of both numerical and experimental analysis for titanium and aluminum alloys are shown in Fig. 10 and 11 respectively. The numerical model predicted failure points for titanium alloy at half way through the height of the specimen, and for aluminum alloy at the top of the specimen, which corresponds well with the experimental results. The final fracture results of both numerical and experimental analysis for titanium and aluminum alloys are shown in Figs. 12 and 13 respectively. The experimental and numerical result show that the material failure occurs at the bottom of the specimen.

The other type of failure which has been observed is wrinkling. There are a number of reasons for wrinkling: die entrance radius is too large, the oil pressure is not enough, too small blank holder pressure (i.e. oil pressure is not enough) and lubrication. One would expect less wrinkling because of rigidity of the floating disk and its ironing effects. Figs. 14 and 15 show the resulting deformed shape of these two alloys sheet. It is clear that the numerical model correctly predicts the wrinkling behavior of these two alloys.

The main goal of the numerical analysis was to verify the predictions of the hydroforming model for these two alloys. As can be seen in these figures the FEM predicted both the wrinkling and fracture modes in this process; therefore, costly experiments can be avoided using a suitable FEM model.

5. Conclusion

Based upon experimental and numerical results the following conclusions are drawn:

1. Titanium alloy, Ti6Al4V and aluminum alloy, Al6016-T6 sheets was successfully formed using hydroforming deep drawing die assisted by floating disc. The advantages of this novel tooling are; normal blank holding force and chamber pressure are halved, punch force is decreased and costs are reduced due to the simplification of the tools and processes.
2. Tensile tests results on Ti6Al4V and Al6016-T6 sheets shows the average values for strain-hardening (n) and strain-rate sensitivity (r) are (0.145, 3.02) and (0.17, 0.57) respectively.
3. Thickness, the yield and tensile strength, strain-hardening and strain-rate sensitivity have effects on forming limit diagram obtained experimentally. As values of n and r increase, the final strain value increases, and as a result, the ultimate elongation increases. This also allows the FLD to shift up.
4. Finally, close agreement is achieved between the experiment and numerical results for these materials. Costly experiments can therefore be avoided using a suitable FEM model; moreover, a better fracture initiation prediction was obtained using Hill-Swift model.

References

[1] Lang LH, Wang ZR, Kang DC, Yuan SJ, Zhang SH, Danckert J, et al. Hydroforming highlights: sheet hydroforming and tube hydroforming. J Mater Process Technol 2004;151:165–77.
[2] Parsa MH, Darbandib P. Experimental and numerical analyses of sheet hydroforming process for production of an automobile body part. J Mater Process Technol 2008;198:381–90.
[3] Zampaloni M, Abedrabbo N, Pourboghrat F. Experimental and numerical study of stamp hydroforming of sheet metals. Int J Mech Sci 2003;45:1815–48.
[4] Yossifon S, Tirosh T. On the permissible fluid-pressure path in hydroforming deep drawing processes – analysis of failures and experiments. Trans ASME J Eng 1988;110:146–52.
[5] Tirosh T, Yossifon S, Eshel R, Betzer A. Hydroforming process for uniform wall thickness products. Trans ASME 1977;99:685–91.
[6] Dieter GE. Mechanical metallurgy. London: McGraw-Hill; 1988. p. 295–301.
[7] Kumar DR. Formability analysis of extra-deep drawing steel. J Mater Process Technol 2002;130:31–41.
[8] Keeler SP. Determination of forming limits in automotive stampings. Sheet Metal Ind 1965;42:683–91.
[9] Goodwin GM. Application of strain analysis to sheet metal forming problems in the press shop. Metal Ital 1968;60:764–74.
[10] Narayanasamy R, Sathiya Narayanan C. Forming, fracture and wrinkling limit diagram for if steel sheets of different thickness. Mater Des 2008;29:1467–75.
[11] Ahmadi S, Eivani AR, Akbarzadeh A. Experimental and analytical studies on the prediction of forming limit diagrams. Comput Mater Sci 2009;44:1252–7.
[12] Stoughton TB, Zhu X. Review of theoretical models of the strain-based FLD and their relevance to the stress-based FLD. Int J Plast 2004;20:1463–86.
[13] Hecker SS. Simple technique for determining forming limit curves. Sheet Metal Ind 1975;5:671–6.
[14] Tadros AK, Mellor PB. An experimental study of the in-plane stretching of sheet metal. Int J Mech Sci 1978;20:121–34.
[15] Gronostajski J, Dolny A. Determination of forming limit curves by means of Marciniak punch. Memories Sci Rev Metal 1980;4:570–8.
[16] Raghavan KS. A simple technique to generate in-plane forming limit curves and selected applications. Metall Trans A 1995;26:2075–84.
[17] Takuda H, Mori K, Hatta N. The application of some criteria for ductile fracture to the prediction of the forming limit of sheet metals. J Mater Process Technol 1999;95:116–21.
[18] Kuroda M, Tvergaard V. Forming limit diagrams for anisotropic metal sheets with different yield criteria. Int J Solids Struct 2000;37:5037–59.
[19] Avila AF, Vieira ELS. Proposing a better forming limit diagram prediction: a comparative study. J Mater Process Technol 2003;141:101–8.
[20] Wang L, Lee TC. The effect of yield criteria on the forming limit curve prediction and the deep drawing process simulation. Int J Mach Tools Manuf 2006;46:988–95.
[21] Swift HW. Plastic instability under plane stress. J Mech Phys Solids 1952;1:1–18.
[22] Hill R. A theory of yielding and plastic flow of anisotropic metals. Proc Roy Soc London 1948;193A:197–281.
[23] Marciniak Z, Kuczynski K. Limit strains in the processes of stretched-forming sheet metal. Int J Mech Sci 1967;9:609–20.
[24] Stren S, Rice R. Localized necking in thin sheets. J Mech Phys Solids 1975;23:421–41.
[25] Holmberg S, Enquist B, Thilderkvist P. Evaluation of sheet metal formability by tensile tests. J Mater Process Technol 2004;145:72–83.
[26] Slota J, Spisak E. Comparison of the forming limit diagram (FLD) models for drawing quality of sheets. Metalurgija 2005;4:249–53.
[27] Shima H, Yang DY. A simple method to determine pressure curve for sheet hydroforming and experimental verification. J Mater Process Technol 2005;167:169–77.